

Theoretical study of the molecular and electronic structure of one-dimensional crystals of potassium iodide and composites formed upon intercalation in single-walled carbon nanotubes

Emma L. Sceats and Jennifer C. Green*

Inorganic Chemistry Laboratory, South Parks Road, Oxford OX1 3QR, United Kingdom

Stephanie Reich

Department of Materials Science and Engineering, Massachusetts Institute of Technology, 77 Massachusetts Avenue, Cambridge, Massachusetts 02139, USA

(Received 1 December 2005; revised manuscript received 6 February 2006; published 30 March 2006)

We report first principles density functional pseudopotential calculations on the molecular and electronic structures of one-dimensional crystals of KI and composites formed upon the intercalation of these ionic crystals within single wall carbon nanotubes (SWNT). For a series of $K_{24}I_{24}$ @SWNT composites the influence of the diameter and chirality of the SWNT on the structures of the 2×2 KI crystals is discussed. The calculated I-I interplanar spacings along and across the KI crystal in the KI@(10,10) composite (3.40 Å and 3.66 Å, respectively) were in good agreement with the experimental lattice measurements reported by Sloan *et al.* [3.46(0.03) Å and 3.98(0.31) Å] for 2×2 KI encapsulated within a SWNT of similar diameter [Chem. Phys. Lett. **329**, 61 (2000)]. The energy of intercalating $K_{24}I_{24}$ within a SWNT was calculated and a Mulliken population analysis was performed for each of the four composites considered here. These Mulliken analyses indicate that a small amount of charge transfer occurs from the SWNT to the KI crystal and that the extent of this charge transfer is dependent on the diameter of the confining nanotube. The intercalation energies exhibit a similar dependency on the diameter of the confining nanotube, with insertion of the 2×2 crystal of KI becoming increasingly exothermic upon reduction of the nanotube diameter from ~ 1.36 nm to ~ 1.10 nm.

DOI: [10.1103/PhysRevB.73.125441](https://doi.org/10.1103/PhysRevB.73.125441)

PACS number(s): 73.21.-b, 68.65.-k, 73.22.-f, 31.15.Ar

I. INTRODUCTION

Carbon nanotubes^{1,2} are unique materials that provide an unparalleled example of the interplay between molecular and electronic structure.³⁻⁶ The sensitivity of the electronic properties of carbon nanotubes, especially single wall carbon nanotubes (SWNTs),² towards changes in their molecular structure has been a subject of considerable interest in the scientific community due to the potential application of these materials in silicon-replacement⁷⁻⁹ and other important technologies.¹⁰⁻¹³ Small variations in nanotube diameter and morphology can produce a large change in the band gap which separates valence and conductance states, resulting in a shift of the electrical conductivity from metallic to semiconducting (and vice versa).^{6,14} In the absence of synthetic protocols for the preparation of SWNTs with a specified diameter, morphology and hence conductivity, other means have been sought to provide bulk samples of SWNTs with electronic properties which have been tailored for a particular application. Chemical manipulation of the electronic properties of SWNTs via *n*-type or *p*-type doping with alkali metals,¹⁵⁻¹⁸ bromine/iodine,¹⁹⁻²² organic and organometallic compounds,²³⁻²⁶ and other materials,²⁷⁻³³ has been studied both experimentally and theoretically. Modulation of the electronic properties of SWNTs has also been achieved through encapsulation of materials in the hollow cavity of the tubes. Notably, Smith *et al.* demonstrated the filling of SWNTs with a fullerene (C₆₀) to form a so-called carbon peapod.³⁴⁻³⁶

In addition to the molecular filling of SWNTs, the central cavity of carbon nanotubes has been shown to serve as a

template for the controlled growth of one dimensional (1D) crystals³⁷ of alkali/alkaline-earth metal oxides/halides, lanthanide oxides/halides, transition metals³⁸ (TM) and TM oxides/halides.³⁹⁻⁴¹ For example, SWNTs may be filled in high yield with KI (Refs. 37, 42, and 43) through a capillary filling method.^{38,40} High resolution transmission electron microscopy (HRTEM) experiments in combination with a through-focal image restoration procedure^{37,44,45} have been used to obtain detailed structural information about these composites and indicate that the structure of the encapsulated salt is dependent upon the diameter of the confining SWNT. It has been shown that individual KI crystals form within the cavities of the SWNTs and can exhibit lengths up to the micrometer range, with the rocksalt <001> direction parallel to the nanotube major axis.⁴³ Filling SWNTs of ~ 1.36 nm in diameter results in the formation of a 2×2 crystal of KI in which the lattice spacing between planes of I ions have been measured. The lattice spacing along the tube axis (3.46 ± 0.03 Å) was found to be similar to that between the <002> planes of bulk (fcc) KI (3.497 Å) but the I-I plane spacing across the SWNT capillary (3.98 ± 0.31 Å) was greater by $\sim 15\%$.⁴³

In contrast to molecularly filled or doped SWNT composites, few reports exist on the use of theoretical methods in the analysis of the molecular and electronic structure of 1D crystals encapsulated in SWNTs.⁴⁶⁻⁴⁹ Possible explanations for the absence of such studies from the scientific literature arise from the difficulties inherent in modeling these systems, which may in part be attributed to the incommensurate periodicities of the solid phase filling and the SWNT. In prepar-

ing a suitable model of the SWNT composite, the need to use a realistic supercell, i.e., one in which the molecular structure of the solid phase filling closely resembles an experimentally determined structure, must be balanced by the need to keep the size of the supercell within computationally-practical limits. The use of empirical, molecular dynamics or other low-level methods enables the study of much larger supercells than is usually feasible in first principles calculations, however, insight into the electronic structure is not normally available from such calculations.

In this paper, we investigate the properties of 1D crystals of KI encapsulated within SWNTs, specifically the 2×2 KI@SWNT composite. This study makes use of advances in linear-scaling methods^{50–53} for density functional theory (DFT) calculations to perform total energy calculations on large supercells (~ 600 – 900 atoms) of 2×2 KI@SWNT. The aim of this research is to extend the scope of previous empirical⁴⁸ and density functional⁴⁶ calculations through an *ab initio* investigation of the molecular and electronic structures of these composites. The availability of detailed structural information for the 2×2 KI@SWNT composite makes this an especially attractive system to study.⁴³ Furthermore, the 2×2 KI crystal represents an interesting structure from a theoretical standpoint. Reduction of the coordination from 6:6 in the bulk to 4:4 in the 2×2 KI crystal is observed in the formation of this all-surface structure. It is of interest to what extent the covalent carbon nanotube has a chemical interaction with the ions, or whether the tube simply provides a confined space for the formation of the 1D crystal. Our calculations will provide values of the KI bond distances, which may be reconciled with the measured iodine lattice spacings, and highlight the role of the diameter and structure of the confining SWNT on the structural and electronic modification of the encapsulated 2×2 KI crystal.

This paper commences with full details of the pseudopotentials and basis sets employed herein and demonstrates the validity of the pseudopotential method through an *ab initio* study of the bulk properties of KI (Sec. II). Section III describes calculations on “free” 1D crystals of KI (i.e., in the absence of an encapsulating tube) which were performed in order to identify how the properties of these low dimensional crystals differ with respect to the bulk. Finally, in Sec. IV we report the results of calculations on 2×2 KI@SWNT [SWNT=(8, 8), (14,0), (17,0) and (10,10)] and interpret data for these composites in terms of the molecular and electronic structures of the empty SWNT and the “free” KI crystal. The energetics of encapsulation are presented and Mulliken population analyses are performed to identify the extent of charge transfer in these KI@SWNT composites.

II. COMPUTATIONAL PROCEDURES

In order to investigate the structural and electronic properties of 1D crystals of KI encapsulated within SWNTs, *ab initio* total energy calculations based on DFT (Refs. 54–56) were performed. All calculations were completed using the SIESTA code, which uses the conjugate gradients minimization method to solve the standard Kohn-Sham (KS) equations.⁵⁷ Minimization of the energy functional was per-

TABLE I. Reference configuration and cutoff radii (a.u.) of the K, I, and C pseudopotentials. For K, an ionic (+1) pseudopotential was generated to enable the inclusion (within the Troullier-Martin scheme) of semicore $3s$ and $3p$ orbitals. I and C pseudopotentials were generated for the neutral atoms.

Reference		K	I	C
		$3s^2 3p^6 3d^0 4f^0$	$5s^2 5p^5 5d^0 4f^0$	$2s^2 2p^2 3d^0 4f^0$
Core radius (a.u.)	s	1.25	1.80	1.25
	p	1.30	1.90	1.25
	d	1.60	3.00	1.25
	f	3.75	2.10	1.25
Core cutoff (a.u.)		1.70	3.50	1.50

formed by diagonalizing the Hamiltonian to find the eigenvalues and eigenfunctions. The exchange and correlation terms were modeled using the generalized gradient approximation (GGA) parameterized by Perdew, Burke, and Ernzerhof.⁵⁸ The electronic density, Hartree and exchange correlation potentials as well as the corresponding matrix elements between the basis orbitals, were calculated using a uniform real-space grid. An equivalent plane wave cutoff between 250–350 Ry was used to represent the charge density in all calculations. In order to perform SIESTA calculations on the systems considered in this study, a number of important points were addressed. These include (i) transferability and convergence of the pseudopotentials, (ii) shape and range of the basis functions, and (iii) convergence of total energies with respect to the \mathbf{k} -point sampling set size and the equivalent plane wave cutoff representing the charge density. Each of these points is addressed for calculations described herein.

A. Pseudopotentials and basis sets (Ref. 59)

The computational expense of performing self-consistent optimization of the KS orbitals for each of the electrons in the unit cell (u.c.) can be reduced through the use of pseudopotentials^{60,61} to model the energetically deep-lying and chemically most inert core electrons. Pseudopotentials have been successfully applied in *ab initio* calculations on a range of systems and the validity of this method is now well established.⁶² Within the SIESTA code, core electrons are replaced by nonlocal, norm-conserving, fully separable Troullier-Martin pseudopotentials,⁶³ whereas valence electrons are described within the linear combination of atomic orbitals (LCAO) approximation. The reference electronic configuration, cutoff radius and partial core cutoff radius for K, I, and C pseudopotentials are included in Table I. The following discussions will focus on the optimization and testing of the K and I pseudopotentials and basis sets.

Due to the large overlap between semicore and valence states in potassium,⁶⁴ the $3s$ and $3p$ orbitals were explicitly included in the calculation. Neglect of ($3s, 3p$) correlation in alkali metal halides, oxides, and hydroxides has previously been shown to result in dramatic failures of *ab initio* calculations to predict correctly structural and thermochemical

data for these compounds.^{65–67} For both K and I, a partial-core correction was included to account for nonlinearity of the exchange and correlation potential between core and valence charge densities.⁶⁸ The I pseudopotential was generated scalar relativistically.

A pseudopotential with good transferability will reproduce the all-electron energy levels and wave functions in arbitrary environments (i.e., in the presence of charge transfer which always takes place in the formation of solids and molecules). A quantitative measure of the quality of a pseudopotential may be obtained by performing all-electron and pseudocalculations on the same series of atomic configurations and comparing the eigenvalues and excitation energies. Cross-excitation energies for both K and I pseudopotentials were not more than 0.14 eV and typically around 0.03–0.04 eV, indicating the excellent transferability of these pseudopotentials.

The one-electron KS eigenstates were expanded using linear combinations of localized numerical atomic orbitals (NAOs).⁶⁹ Multiple- ζ , split valence bases were employed for both K and I. A double- ζ (DZ) basis set was used for the semicore and valence states of K ($3s, 3p, 4s$) and I ($5s, 5p$). Polarizing and diffuse functions were added to the basis set to enable sufficient flexibility in the shape and range of the orbitals. This flexibility is especially important for ionic systems in which the valence orbitals of cations (anions) tend to shrink (expand). The bases were augmented with single- ζ (SZ) ($4p$) and ($6s, 5d$) functions, and DZ $3d$ and $6p$ diffuse functions for K and I, respectively. The localization of NAOs, essential to their application in linear-scaling calculations, was enforced within a soft confinement potential.⁶⁹ This scheme provides a “softer” approach to that described by Sankey *et al.* in which strict localization of basis orbitals beyond a core cutoff radius r_c has the effect of creating a discontinuity in the derivative.⁷⁰ This discontinuity is more pronounced for orbitals that would be quite extended in the free atom, resulting in errors in the calculated total energy, forces, and stresses on the atoms. This softer localization scheme also has the advantage of increased efficiency with respect to the soft confinement methods suggested by Porezag⁷¹ and Horsfield.⁷² Parameters defining the shape and range of the basis functions were obtained by variational optimization in bulk (fcc) KI, following the procedure defined by Junquera.⁶⁹

B. *Ab initio* calculations on bulk (fcc) KI

In order to establish the quality of the pseudopotentials and basis sets, optimized for K and I, an intensive study of bulk face centered cubic (fcc) KI was performed. For KI, the main issues are the transferability of the pseudopotentials into the solid state environment and \mathbf{k} -point convergence. Periodic boundary conditions (PBCs) on the fcc u.c. were used in all calculations. Sampling of reciprocal space was performed using a $(4 \times 4 \times 4)$ Monkhorst-Pack mesh,⁷³ leading to 32 \mathbf{k} -points in the irreducible Brillouin zone (BZ). Increasing the size of the real/reciprocal space mesh produced negligible changes in the total energy of the system ($<1 \times 10^{-3}$ meV).

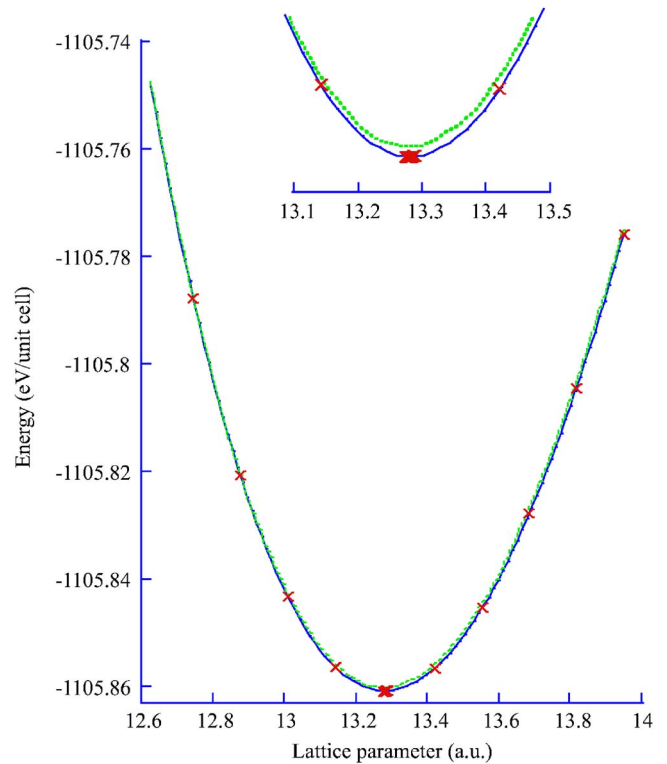


FIG. 1. (Color online) Plot of energy (eV/u.c.) versus lattice parameter (a.u.) for bulk (fcc) KI. Calculated data points are represented by red crosses. Quartic and Murnaghan fits to these data are represented by green (dashed) and blue (solid) lines, respectively.

A cohesive curve for bulk KI was obtained by fitting calculated values of the total energy for fifteen different u.c. volumes ($\pm 5\%$ of the equilibrium volume, V_0) to a quartic equation and the Murnaghan⁷⁴ equation of state (EOS) (Fig. 1).⁷⁵ The Murnaghan EOS may be expressed as

$$\frac{V}{V_0} = \exp \left[-\frac{1}{B'_0} \ln \left(1 + \frac{B'_0 P}{B_0} \right) \right], \quad (1)$$

where V_0 is the u.c. volume at equilibrium, V is the u.c. volume at pressure P , B_0 is the bulk modulus, and B'_0 is the pressure derivative of the bulk modulus. V_0 [and hence the equilibrium lattice constant (a)] (Ref. 76) was obtained by differentiation of the two curves. The calculated value of the lattice constant was found to deviate from the experimental (0 K) data by $\sim 0.5\%$ (calc. 7.029 Å; expt. 6.994 Å),⁷⁷ indicating excellent agreement between this calculation and the experimental data.

The bulk modulus B_0 is defined by Eq. (2),

$$B_0 = V \frac{\delta^2 E}{\delta V^2}, \quad (2)$$

where E is the total ground state energy as a function of volume and B_0 is evaluated at the minimum of E . B_0 given by the quartic (16.06 GPa) and Murnaghan (16.00 GPa) fits to the data deviate from one another by only 0.3%. The Murnaghan data will be used hereafter for comparison with experimental, calculated, and zero-point corrected (ZPC) data.

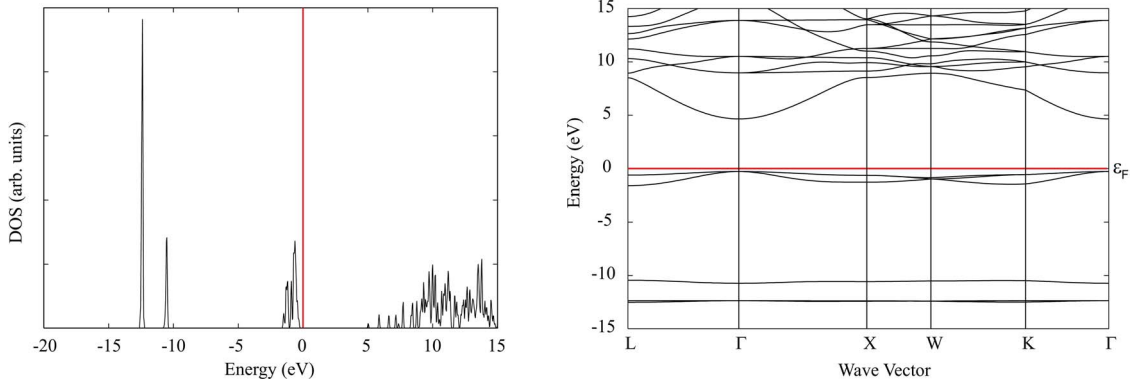


FIG. 2. (Color online) Calculated DOS (left) and electronic band structure (right) for bulk (fcc) KI. The Fermi energy (ϵ_F) is indicated by a solid red line plotted at 0 eV.

Zero-point and finite temperature effects, present in experiments but absent from most calculations, must be accounted for in order to make a fair comparison between experimental and calculated B_0 . Calculation of the ZPC B_0 ($B_{0\text{-ZPC}}$) for bulk KI (using B_0 at 300 K of 12.0 GPa) (Ref. 77) was performed according to the methodology of Gaudoin and Foulkes,⁷⁸ and provided a value of 14.02 GPa.⁵⁹ The calculated B_0 of 16.00 GPa provides an overestimation of $B_{0\text{-ZPC}}$ by 14%. This discrepancy may arise from a number of sources: (i) the shape and range of the basis functions for K and I have been optimized such that attractive interactions in the solid state are slightly overestimated with respect to repulsive interactions. This may be due to the extension of the negative ion charge density which may have been underestimated in our optimized basis for I. (ii) Incorrect treatment of the exchange and correlation functions has previously been shown to have a significant effect on the accuracy of calculated bulk moduli. (iii) It should also be noted that uncertainties in experimental bulk moduli are much greater than for lattice constants and can be as large as 10%–15%.

Band structure and density of states (DOS) calculations were performed for bulk KI at the equilibrium u.c. volume. The band structure of bulk (fcc) KI along the symmetry directions Γ -(Δ)-X-(Z)-W-(Q)-L-(λ)- Γ -(Σ)-K-L (for the NaCl structure) is shown in Fig. 2. The general topology of the calculated band structure is in good agreement with those reported previously⁷⁹ providing further support for the suitability of our optimized pseudopotentials and basis sets. In the energy regime close to the Fermi level (ϵ_F , defined as the top of the highest filled band and energy referenced with respect to the vacuum), which was calculated to be -5.13 eV (but shifted in Fig. 2 to 0 eV), the bands may be assigned as follows (from most negative to most positive): the triplet bands at the bottom of the valence band (energy ca. -13 eV) arise from the $3p^6$ electrons of K; the singlet band (ca. -11 eV) arises from the $5s^2$ electrons of I; the three bands appearing near the Fermi level (-1.5 to 0 eV) arise from the $4s^1$ electron of K and the $5p^5$ electrons of I; the lowest lying states of the conduction band arise from the $4p^0$ and $3d^0$ states of K and the $6s^0$ and $5d^0$ states of I. The calculated band gap of 5.15 eV represents an appreciable underestimation of the experimental band gap (6.2 eV),⁸⁰ however, in the Kohn-Sham model the use of exchange-correlation function-

als, such as those employed herein, systematically results in band separations that are smaller than those measured in experiments. This underestimation is due to the poor description of excited states in which the polarization effect is not accounted for by the usual functionals used in DFT.⁸¹ Since the ground-state properties of these systems are well reproduced in DFT, this error does not affect our conclusions.

III. ONE-DIMENSIONAL KI

Calculations on 1D structures of KI, in the absence of a confining SWNT, were performed in order to understand how the properties of these low dimensional crystals differ with respect to the bulk. These simple (and hypothetical) systems will be used as the benchmark for estimating the importance of the diameter and structure of the confining SWNT on modifying the molecular and electronic structures of SWNT-encapsulated KI crystals.

Full geometry and lattice relaxations were performed on a number of supercells of 2×2 KI. All calculations were performed using the optimized K and I pseudopotentials and basis sets described in Sec. II. Within the framework of the SIESTA program, it is possible to model these 1D crystals as either infinite or molecular systems. Calculations were performed using both methods so that the influence of the modeling method on the results could be ascertained. For the molecular systems a series of geometry optimizations were performed on molecules of stoichiometry $(\text{KI})_{2n+2}$ consisting of n face sharing K_4I_4 units, the aim being to determine the number of units (n) at which structural convergence (quantified by the KI bond length in the central unit) and energetic convergence are achieved (Fig. 3).

PBCs were imposed to model the 2×2 KI crystals as infinite, isolated systems and reciprocal space was sampled with a $(1 \times 1 \times 6)$ Monkhorst-Pack mesh, leading to 4 \mathbf{k} -points in the irreducible Brillouin zone (BZ). PBCs were also imposed to model the 2×2 KI crystals as isolated molecular systems, (reciprocal space sampling at the Γ point) however, the lattice vector in the z -direction was large enough to prevent interaction of the crystal with its periodic images.

Results: Calculated structural parameters (measured at the center unit), energy (per face sharing K_4I_4 unit) and Fermi

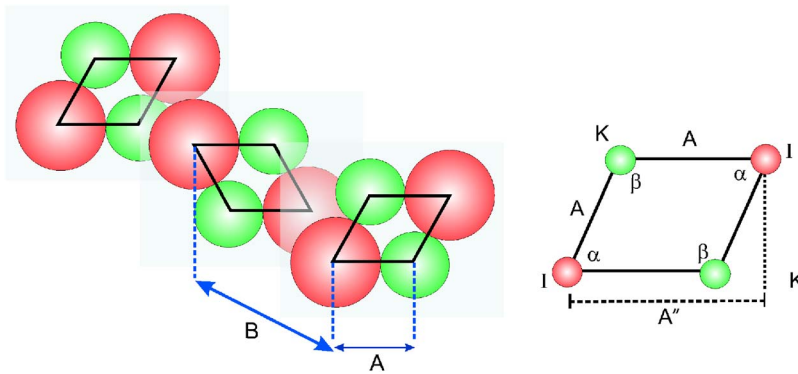


FIG. 3. (Color online) View down the body of a 2×2 crystal of KI showing three K_2I_2 faces, i.e., two face sharing K_4I_4 units (n) (left; K, green; I, red). KI bond lengths A and B are depicted. An expanded view of one K_2I_2 face, showing the angles α (K-I-K) and β (I-K-I), and the I-I plane spacing A'' , is also presented (right).

energy (ϵ_F), for supercells ranging in size from $n=1$ to $n=45$ (modeled as both infinite and molecular systems) are provided in the supporting EPAPS material (Tables SI-5 and SI-6).⁵⁹ Structurally and energetically the calculated models of both the infinite and molecular 2×2 KI crystals are sufficiently well converged for supercells comprising 11 or more face sharing K_4I_4 units ($n \geq 11$).⁸² Thus the results for 11 units will be presented below.

The optimized structure for the infinite 2×2 KI crystal consists of parallel K_2I_2 planes; the K and I ions within the plane (A) form a rhombus with all four KI distances equal (3.416 Å). The K-I-K angle (α) is acute (85.3°) and the I-K-I angle (β) obtuse (94.7°). The KI distance between the planes (B) is slightly shorter (3.388 Å). (Fig. 3 defines the structural parameters.) The cross-sectional area (CSA) of the infinite system is consistent throughout the length of the crystal at 11.64 \AA^2 .

Structural convergence within the molecular systems was tested by comparing the CSA at a number of points along the crystals. For the molecular system, small variations are observed in the CSA at either end of the crystal, however, the CSA is constant in units 4–8, taking a value of 11.63 \AA^2 . As for the infinite system, the K_2I_2 planes form a rhombus (Fig. 3) with K-I-K (α) and I-K-I (β) bond angles of 85.2° and 94.8°.

The KI bond lengths A (3.418 Å) and B (3.388 Å), in the central 5 units of the molecular crystal, were virtually identical to those calculated for the infinite system indicating that the central units of a 2×2 $K_{24}I_{24}$ molecule give a good representation of the structural dimensions of an infinite 2×2 crystal (see Table II). These values are between 2.8% to 3.6% shorter than the KI bond calculated for bulk (fcc) KI

(3.515 Å). Slight expansion of the KI bonds A, compared to KI bonds B is calculated for both molecular and infinite systems and may be quantified by an A/B ratio of 1.01. This finding is in agreement with calculations reported by Wilson,⁴⁸ in which an A/B ratio of 1.03 was attributed to the relative balance of forces on an ion along the z axis and the x and y axes, respectively.

In the molecular system, contraction of KI bonds A (by approximately 3%, to $\sim 3.302 \text{ \AA}$), in units 1 and 11, results in tapering of the crystal at either end. A smaller contraction of around 1% is seen for KI bonds B in the terminal units. This tapering is expected since the coordination of the K and I ions is reduced from 4-coordinate in the body of the 2×2 crystal, to 3-coordinate at the terminal ion positions in the crystal.

The Fermi energies (ϵ_F) calculated for supercells ($1 \leq n \leq 45$) of 2×2 KI [Figure SI-3(b) and Tables SI-2 and SI-3 in EPAPS (Ref. 59)] demonstrate a difference of around 0.2 eV due to the modeling method employed. The calculated ϵ_F of a molecular crystal comprising 11 face sharing K_4I_4 units was -1.05 eV , while for an infinite crystal ($n=11$) ϵ_F was -0.78 eV . Again, this parameter is well converged for larger supercells ($n \geq 11$) with fluctuations typically less than 0.05 eV for both molecular and infinite crystals.

Band structure and DOS calculations were performed on infinite and molecular 2×2 crystals of KI ($n=11$). The calculated electronic band structures and DOS for both crystals were almost identical in their general topologies, and their DOS plots were very similar to the calculated DOS for bulk (fcc) KI. A minor difference was observed in the magnitude of the band gap (E_{gap}) which was slightly larger for the infinite model (6.69 eV) compared to the molecular model

TABLE II. Structural parameters, Fermi energy (ϵ_F , defined as the top of the highest filled band and energy referenced with respect to the vacuum), and band gap (E_{gap}) for molecular and infinite supercells comprising 11 face sharing K_4I_4 units (stoichiometry $K_{24}I_{24}$). Structural parameters are recorded for units 4–8 in both systems. A'' is the I-I plane spacing (across the crystal), α is the K-I-K angle, and β is the I-K-I angle. Standard deviations are provided in parentheses.

	A (Å)	A'' (Å)	B (Å)	A/B	A''/B	α (°)	β (°)	ϵ_F (eV)	E_{gap} (eV)
Molecular	3.418 (0.001)	3.56 (0.012)	3.388 (0.001)	1.009	1.05	85.2	94.8	-1.05	6.45
Infinite	3.416 (0.003)	3.55 (0.017)	3.388 (0.003)	1.008	1.05	85.3	94.7	-0.80	6.69

(6.45 eV). The band gaps for the 1D systems were larger (by $\sim 1.3\text{--}1.5$ eV) than that calculated for bulk KI (5.15 eV).

IV. ONE-DIMENSIONAL KI ENCAPSULATED IN SWNTS

A. KI@SWNT: The model

For solid phase filled SWNT composites such as KI@SWNT, four different modeling methods are available, which depend on the chosen means for applying PBCs to the system. Yam and co-workers have reported calculations on an infinite crystal of KI encapsulated in an infinite SWNT.⁴⁶ In this work, calculations were performed on a supercell comprising a single K_4I_4 unit of 2×2 KI ($A=3.69$ Å, $B=4.0$ Å) and three unit cells of a (10,10) SWNT (overall stoichiometry: $\text{K}_4\text{I}_4\text{C}_{120}$). The chosen supercell represents the smallest realistic supercell of KI encapsulated within a (10,10) SWNT and has the disadvantage of enforcing $\sim 6\%$ increase in the interplanar spacing along the tube, compared with the experimental distance. Furthermore, it is doubtful whether the supercell is of a sufficient length to model accurately a fragment of 2×2 KI@SWNT which is several micrometers in length.

The primary problem with modeling systems such as KI@SWNT via an infinite crystal/infinite SWNT approximation arises from the incommensurate periodicity of the SWNT unit cell with the unit of the 2×2 KI crystal. Ideally, the translational component in the z direction (T_z) would be chosen as the smallest common multiple of the SWNT unit cell and the K_4I_4 face sharing unit length for which N units of 2×2 KI are encapsulated within M unit cells of SWNT. Unfortunately, this method is often impractical due to the computational expense of working with such large supercells (1000s of atoms). More commonly, and in the case of calculations performed by Yam *et al.*, the supercell of a filled SWNT is constructed such that the periodicity of one component (usually the filling material) is altered to match that of the other component and to afford (overall) a smaller translational vector.⁴⁶ Given the intimate relationship between structural and electronic properties, an obvious disadvantage of this method is the inevitable modification of the electronic properties of the composite. Furthermore, expansion (or contraction) of the KI crystal or SWNT, in the direction of the principal axis, is to some extent limited by the PBCs.

Alternatively, both the KI crystal and the SWNT can be treated as molecules. For the SWNT this can be achieved by either capping the tube with the hemisphere of a suitable fullerene, or by saturating the dangling bonds at either end of the tube with suitable functional groups (e.g., H, F, COH, CO_2H). This modeling method was rejected since the choice of capping/functional group has previously been shown to influence the molecular and electronic structures of SWNTs quite considerably.⁸³ Also, there exists the possibility of interactions between the capping/functional group and the KI crystal and the influence of these end effects on the energetic and structural data would be difficult to quantify and would undoubtedly depend on the chosen method for terminating the SWNT.

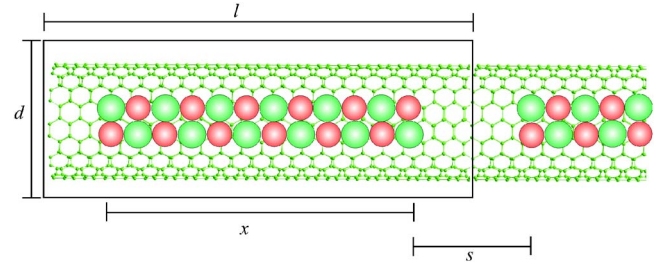


FIG. 4. (Color online) Model of 2×2 KI@SWNT; specifically, a molecular crystal of $\text{K}_{24}\text{I}_{24}$ (green and red spheres) encapsulated within 21 unit cells of (10,10) SWNT (not to scale). Structural parameters for this model are defined as follows: l defines the overall length of the supercell, d defines the depth of the supercell, x defines the length of the 2×2 KI crystal, and s defines the separation between terminal ions in neighboring $\text{K}_{24}\text{I}_{24}$ crystals.

Our chosen method for modeling 2×2 KI@SWNT utilizes a supercell constructed from an infinite section of a SWNT filled with a molecular crystal of 2×2 $\text{K}_{24}\text{I}_{24}$ (Fig. 4, Table III). A similar model has previously been employed in calculations reported by Wilson.⁴⁹ Our calculations on “free” 2×2 KI (Sec. III) have shown that the central units of a 2×2 $\text{K}_{24}\text{I}_{24}$ molecule give a good representation of the structural dimensions of an infinite 2×2 crystal. By modeling the SWNT as an infinite system, end effects due to interaction of the KI crystal with capping/functional groups are avoided and it is possible to perform a direct comparison between encapsulated crystals of 2×2 KI and “free” 2×2 KI crystals. The supercells of 2×2 KI@SWNT have been constructed to ensure that the $\text{K}_{24}\text{I}_{24}$ crystal cannot interact with its periodic images in neighboring unit cells. This is achieved by encapsulating the KI crystal within a large supercell of a SWNT such that at either end of the system there is a segment of SWNT which is unfilled (Fig. 4). Modeling the KI crystal as a molecular species enables greater flexibility in the positioning of the ions with respect to the carbon atoms of the tube wall, and allows for expansion/contraction of the encapsulated KI crystal along the nanotube axis. Relevant structural parameters for the models employed in calculations on KI@SWNT [SWNT=(8,8), (14,0), (17,0), and (10,10)] are summarized in Table III.

The SWNTs chosen in this study will enable the effects of both the diameter (d_t) and structure of the nanotube, on the molecular and electronic structure of the encapsulated KI

TABLE III. Structural parameters for models of $\text{K}_{24}\text{I}_{24}$ @SWNT: d_t is the diameter of the (empty) SWNT; n is the number of face sharing K_4I_4 units. “Atoms” gives the total number of atoms in the composite.

SWNT	d_t (Å)	Number of u.c. SWNT	l (Å)	n	x (Å)	s (Å)	Atoms
(8,8)	10.85	20	49.1	11	37.2	12.0	688
(14,0)	10.96	12	51.1	11	37.2	13.9	720
(17,0)	13.31	12	51.1	11	37.2	13.8	884
(10,10)	13.56	21	51.6	11	37.2	14.5	888

TABLE IV. Structural and energetic data for $K_{24}I_{24}@SWNT$. The energy change of the distorted $K_{24}I_{24}$ crystals $\Delta E(K_{24}I_{24})$, with respect to the ground state structures, is calculated as follows: $[-E_{TOTAL}(\text{free KI}) + E_{TOTAL}(\text{distorted KI})]$ (units, meV/KI). The energy change of the distorted SWNT $\Delta E(SWNT)$, with respect to the ground state structure, is calculated as follows $[-E_{TOTAL}(SWNT) + E_{TOTAL}(\text{distorted SWNT})]$ (units, meV/C atom). The intercalation energy of the $K_{24}I_{24}@SWNT$ composites is defined as $\{-E_{TOTAL}(KI@SWNT) + [E_{TOTAL}(\text{free KI}) + E_{TOTAL}(SWNT)]\}$ (units, meV/KI). The lattice parameter (l , Å) of the ground state and distorted SWNTs are also provided.

	KI@(8,8)	KI@(14,0)	KI@(17,0)	KI@(10,10)
$\Delta E(K_{24}I_{24})$ (meV/KI)	+110	+92	+4.2	+10
Z_{SWNT} (Å)	49.13	51.06	51.06	51.61
$Z_{\text{distorted}SWNT}$ (Å)	49.14	51.07	51.07	51.62
$\Delta E(SWNT)$ (meV/C atom)	+1.03	+0.77	+0.08	+0.11
Intercalation energy (meV/KI)	-367	-399	-253	-223

crystal, to be investigated. Furthermore, in the case of 2×2 KI@ (1.36 nm SWNT), a direct comparison can be made between the calculated lattice spacings and experimentally measured distances for this system.⁴³ For each KI@SWNT composite (listed in Table III), a full geometry and lattice optimization was performed (1 \mathbf{k} -point, 250 Ry) until the residual forces were less than 0.06 eV/Å and the stress tensor was below 0.02 GPa. Geometry and lattice optimizations were also performed on each of the (empty) SWNT supercells and full details of these calculations can be found in the supporting EPAPS material.⁵⁹ Following structural optimization of each composite, single point calculations were performed on the distorted empty SWNT and the distorted “free” KI crystal. Structural and energetic data for all of these calculations are listed in Table IV.

B. Results and discussion

Subsequent to optimization of the KI@SWNT composites, a detailed structural analysis of the distorted 2×2 KI

crystal was performed. Significantly, for the KI@(17,0) and KI@(10,10) composites, this study demonstrates the first theoretical treatment of a solid phase filled SWNT in which good agreement is found with the experimental I-I lattice spacings for a 2×2 crystal of KI encapsulated in a SWNT of a similar diameter (Table V).

For each composite, the average KI bond lengths A and B, the I-I plane spacing across the 2×2 KI crystal (A''), the ratios A/B and A''/B , and the angles α and β , for units 4–8 (inclusive), are summarized in Table V. In general for the encapsulated crystals, the KI bond lengths along the crystal (B) (in units 4–8) show relatively little variation, regardless of the diameter of the confining SWNT (d_t). In the “free” 2×2 (molecular) crystal of KI the average KI bond length B is 3.388 Å, while for the encapsulated crystals B varies between 3.38 Å and 3.40 Å. In contrast, the average KI bond length A for the KI@SWNT composites varies over a much larger range and the magnitude of A can be directly correlated with d_t . Specifically, as the diameter of the confining

TABLE V. Calculated average bond lengths and angles for units 4–8 in (i) a supercell comprising 11 face sharing K_4I_4 units ($K_{24}I_{24}$), and (ii) $K_{24}I_{24}@SWNT$ [SWNT=(8,8), (14,0), (17,0), and (10,10)]. A is the KI bond length across the crystal, A'' is the I lattice spacing across the crystal, and B is the KI bond length along the crystal. Standard deviations are reported in parentheses. Angles α and β are the K-I-K and I-K-I angles, respectively. Experimental bond distances taken from Ref. 43 are given for KI@(1.36 nm SWNT). Italicized values enclosed in square brackets (e.g. [1.03]) are calculated A/B ratios taken from Ref. 48.

	A (Å)	A'' (Å)	$(A''-A)$ (Å)	B (Å)	A/B	A''/B	α (°)	β (°)	$(90-\alpha)$ (°)
$K_{24}I_{24}$	3.42 (0.001)	3.56 (0.012)	+0.14	3.39 (0.001)	1.01 [1.03]	1.05	85.2	94.8	4.8
KI@(8,8)	3.30 (0.004)	3.08 (0.006)	-0.22	3.38 (0.006)	0.98 [0.92]	0.91	96.8	83.2	-6.8
KI@(14,0)	3.32 (0.008)	3.13 (0.009)	-0.19	3.39 (0.015)	0.98	0.92	96.2	83.8	-6.2
KI@(17,0)	3.48 (0.033)	3.65 (0.046)	+0.17	3.41 (0.005)	1.02	1.07	84.0	96.0	6.0
KI@(10,10)	3.49 (0.003)	3.66 (0.011)	+0.17	3.40 (0.002)	1.03 [1.05]	1.08	83.7	96.3	6.3
KI@(1.36 nm SWNT)		3.98 (0.31)		3.46 (0.03)		1.15			

SWNT increases in the order $(8,8) < (14,0) < (17,0) < (10,10)$, the magnitude of A increases from 3.30 \AA to 3.49 \AA .

Intercalation of 2×2 KI in a SWNT for which $d_t \approx 1.36 \text{ nm}$ [i.e., $(10,10)$ and $(17,0)$ SWNTs] causes minor structural changes compared to the “free” crystal of KI. The lack of strain invoked in the 2×2 crystal of KI upon its intercalation in a 1.36 nm diameter SWNT is evident in the negligible increase in energy for the distorted crystal [$\Delta E(K_{24}I_{24}) = 4.2 \text{ meV/KI}$ for KI@ $(17,0)$ and 10 meV/KI for KI@ $(10,10)$] compared to the fully optimized structure (Table IV). The encapsulated crystal exhibits tapering in the terminal units of a similar magnitude to that seen in the “free” crystal ($\sim 1\%$ for KI bonds B and $\sim 3\%$ for KI bonds A). Through the middle section of the KI crystal (units 4–8), elongation of the KI bonds A ($\sim 2\%$), across the nanotube capillary, results in an A/B ratio of 1.02 for KI@ $(17,0)$ and 1.03 for KI@ $(10,10)$. This increase in the A/B ratio upon encapsulation in a $(10,10)$ SWNT is similar to that predicted by Wilson.⁴⁸ In Wilson’s article, Born-Mayer and Lennard-Jones potentials were used to model the ion-ion and ion-carbon interactions, and calculations on “free” 2×2 KI and 2×2 KI@ $(10,10)$ (see italicized entries e.g., [1.05], Table V) demonstrated that bond expansion across the 1D KI crystal was the result of ion-carbon separations lying on the attractive side of the Lennard-Jones potential minimum. Thus, outward expansion of the 2×2 KI crystal, towards the wall of the SWNT, is favored in the minimum energy structure.

From the calculated structure of $K_{24}I_{24}@ (10,10)$ it is possible to estimate the distance between the I lattice planes both along and across the tube. It is this I-I lattice spacing that has been measured by TEM on a 2×2 KI crystal intercalated in a SWNT of diameter 1.36 nm . The I-I interplanar spacing along the tube is equivalent to the KI distance B and thus the value for B of 3.40 \AA is in good agreement with the experimental measurement of $3.46(0.03) \text{ \AA}$. Due to the rhombic shape of the K_2I_2 units, the experimental I-I lattice spacing across the tube, $3.98(0.31) \text{ \AA}$ should be compared with the calculated A'' , 3.66 \AA (Fig. 3, Table V) thereby giving a reasonable agreement when the standard deviation on the experimental measurement is taken into account. Though the I-I lattice spacings for KI@ (1.36 nm SWNT) are slightly shorter than those observed experimentally,⁴³ this may in part be attributable to zero-point and finite temperature effects that are present in experiments but absent from these calculations.

Intercalation of 2×2 KI in a SWNT for which $d_t \sim 1.10 \text{ nm}$ [i.e., $(8,8)$ and $(14,0)$ SWNTs] results in more significant structural distortion of the encapsulated crystal. The increase in strain for the distorted 2×2 crystals of KI from the KI@ $(8,8)$ and KI@ $(14,0)$ composites is evident in the large increase in energy [$\Delta E(K_{24}I_{24}) = 110 \text{ meV/KI}$ and 92 meV/KI , respectively] compared to the fully optimized structures (Table IV). As for the KI@ (1.36 nm SWNT) composites, the KI bond lengths B ($\sim 3.38 \text{ nm}$) along the crystal show relatively little change upon intercalation in SWNTs for which $d_t \sim 1.10 \text{ nm}$. The most significant structural change that occurs upon encapsulation of the 2×2 KI crystals in these smaller diameter SWNTs is a contraction of the

KI bonds A, across the nanotube capillary, by $\sim 3.5\%$. This decrease in A results in reduction of the A/B ratio from 1.01 in the “free” crystal to 0.98 , and for the KI@ $(8,8)$ composite, this calculated A/B ratio is slightly larger than predicted by Wilson (0.92).⁴⁸ The reduction in A is accompanied by an increase in the K-I-K bond angle (α) to between 96° – 97° and a decrease in the I-K-I bond angle (β) to between 83° – 84° . In contrast to KI@ (1.36 nm SWNT) , KI crystals in these composites exhibit insignificant tapering in the terminal K_4I_4 units, probably as a result of the large strain/energy increase that would result upon forcing similarly charged ions into closer proximity.

Analysis of structural data for the KI@SWNT composites reveals that as the diameter of the SWNT decreases [$(10,10) > (17,0) > (14,0) > (8,8)$], the value of $(90 - \alpha)$ increases. For the wider diameter $(17,0)$ and $(10,10)$ SWNTs, in which $\alpha < 90^\circ$, A'' provides an *overestimation* of the KI bond length A by 0.17 \AA . However, for the narrower diameter $(8,8)$ and $(14,0)$ SWNTs, in which $\alpha > 90^\circ$, A'' provides an *underestimation* of the KI bond length A by 0.22 \AA and 0.19 \AA , respectively.

Interestingly, despite utilizing almost identical supercells of KI@SWNT the optimized structures calculated in this work failed to reproduce the twisting of the 2×2 KI crystals that was reported by Wilson.⁴⁹

Analysis of the SWNT in each KI@SWNT composite revealed that negligible structural distortions occur upon filling with KI. For the larger diameter $(10,10)$ and $(17,0)$ SWNTs, the distortions accounted for an increase in energy [$\Delta E(\text{SWNT})$] of $\sim 0.1 \text{ meV}$ per C atom compared to the ground state energy of the nanotube (Table IV). For the smaller diameter $(8,8)$ and $(14,0)$ SWNTs, the strain induced in the nanotube upon filling resulted in a slightly larger increase in the energy [$\Delta E(\text{SWNT})$] of $\sim 1.0 \text{ meV}$ per C atom. The lattice length of the SWNTs, regardless of the diameter, showed an increase of $< 0.01 \text{ \AA}$ ($\sim 0.02\%$) upon filling with KI, suggesting that the axial strain invoked upon filling is negligible.

For each of the KI@SWNT composites, a comparison of the Mulliken population analysis for the “free” KI crystal, the empty SWNT, and the composite was used to determine the extent of charge transfer from/to the SWNT and the KI crystal (Table VI).

Overall, the KI@SWNT composites showed negligible charge transfer between the SWNT and the ionic KI filling. For all composites, filling with KI results in a decrease of the electron density in the SWNT and a concomitant increase in the electron density of the ionic crystal. The magnitude of the decrease for the SWNT is seen to depend upon d_t , with smaller diameter SWNTs demonstrating a greater degree of charge transfer compared to wider diameter nanotubes. In this study, KI@ $(8,8)$ and KI@ $(14,0)$ exhibited the largest amount of charge transfer from the SWNT, with 1.79 electrons ($2.8 \times 10^{-3} e^-$ per C atom) and 1.62 electrons ($2.4 \times 10^{-3} e^-$ per C atom) respectively transferred from the nanotube. According to Sun *et al.*,⁸⁴ the bond shrinking resulting from this reduction in the electronic density of the SWNT would account for an overall negative length strain in the SWNT of $< 0.1\%$. This prediction is in agreement with

TABLE VI. Changes in measured charge distribution for KI@SWNT composites, compared to an empty SWNT and a “free” 2×2 crystal of KI. Values in parentheses represent electrons per atom/ion.

Composite	Charge distribution			
	K	I	KI (total)	SWNT
KI@(8,8)	0.31 (0.013)	1.44 (0.06)	+1.75	-1.79 (2.8×10^{-3})
KI@(14,0)	0.12 (0.005)	1.06 (0.06)	+1.63	-1.62 (2.4×10^{-3})
KI@(17,0)	-0.07 (-0.003)	0.49 (0.02)	+0.42	-0.42 (0.5×10^{-3})
KI@(10,10)	-0.06 (-0.003)	0.26 (0.01)	+0.19	-0.18 (0.2×10^{-3})

the calculated structures of these composites, which show negligible changes in the overall length of the SWNT lattice upon intercalation of KI. KI@(17,0) and KI@(10,10) exhibit a much smaller degree of charge transfer, with 0.18 electrons ($0.2 \times 10^{-3} e^-$ per C atom) and 0.42 electrons ($0.5 \times 10^{-3} e^-$ per C atom) removed from the (10,10) and (17,0) SWNTs, respectively.

Changes in the electron density of the KI crystal upon intercalation in a SWNT result primarily from charge transfer from the SWNT to the iodide ions of the ionic crystal. In all of the composites, the K ions exhibit negligible changes in their charge density due to the cationic (+1) pseudopotential employed in these calculations. Previous experimental work^{19,20} and density functional calculations^{21,22} on halogen-doped SWNTs have demonstrated similar trace quantities of charge transfer from the SWNT to the halogen atoms. Recent calculations by Yam *et al.* on KI@(10,10) provided evidence for a complex charge transfer process in which both the SWNT and the KI crystal exhibited a reduction in their electronic densities, while a simultaneous increase was observed in the electronic density in the interstitial region between the nanotube and the ionic crystal.⁴⁶ Yam reported that one in four potassium 4s electrons are transferred to the nanotube wall and 0.3 e^- per C atom are transferred from the nanotube to the KI-SWNT interstitial region. While the magnitude of charge transfer from the K ions cannot be analyzed in the present work, our calculations suggest that the extent of charge transfer from the SWNT is less significant than was predicted by Yam and co-workers. Furthermore, our calculations give evidence for accumulation of the electron density, which was removed from the SWNT, on the iodide ions of the KI crystal.

Finally, data for both KI@(1.36 nm SWNT) and KI@(1.10 nm SWNT) suggest that the structure (armchair or zig-zag) and conductivity (metallic or semiconducting) of the confining SWNT are less important in controlling the molecular and electronic structure of the ionic intercalate than the diameter (d_t) of the nanotube. Interestingly, despite increased strain in the ionic filling upon reducing the diameter of the SWNT, the intercalation of these 2×2 KI crystals within the narrow diameter ($d_t \sim 1.10$ nm) nanotubes is more thermodynamically favorable than their insertion into the larger diameter ($d_t \sim 1.36$ nm) SWNTs. In the KI@(10,10) and KI@(17,0) composites the intercalation energies are very similar at -223 meV/KI and -253 meV/KI, respectively. However, for the KI@(8,8) and KI@(14,0) composites the intercalation energies are more exothermic at

-367 meV/KI and -399 meV/KI, respectively. The increased exothermicity accompanying intercalation of the KI crystals into the (8,8) and (14,0) SWNTs is primarily attributed to the increased charge transfer from the SWNT to the KI when the crystal is encapsulated within the smaller diameter nanotubes.

V. CONCLUSION

The molecular and electronic structures of a series of KI@SWNT composites have been investigated using density functional calculations. The crystals consist of parallel K_2I_2 planes with the four atoms forming a rhombus. The KI bond length A and the K-I-K angle α were shown to demonstrate a proportional and inverse dependence respectively on the diameter of the encapsulating SWNT. This study demonstrates a theoretical description of 2×2 KI@(1.36 nm SWNT) in which good agreement is achieved with the I-I lattice spacings measured in HRTEM experiments.

Additionally, analysis of the charge distribution for each KI@SWNT composite confirmed that a small amount of charge transfer occurs between the ionic filling and the SWNT, and the extent of the charge transfer was seen to depend on the diameter of the confining nanotube. In contrast with previous reports, we find that changes in the electron density of the KI crystal upon intercalation in a SWNT result primarily from charge transfer from the SWNT to the iodide ions of the ionic crystal.

Understanding the interactions that occur between solid phase filling materials, such as KI, and a confining SWNT, is relevant for the application of these composites in molecular electronic devices, and for the chemical or structural manipulation of these systems. Potentially, the chemical reactivity of the SWNT may be modified (compared to the pristine, empty SWNT) upon filling, thus changing the propensity with which functional groups can be appended to the outer wall, or altering the solution-based behavior of the composite.

Application of the methodology outlined in this article, in the theoretical analysis of related KI@SWNT composites, and other solid phase filled SWNT composites is currently being pursued in our laboratories. In addition, the structural information obtained from our theoretical calculations on the 2×2 KI@SWNT composites has prompted fresh experimental efforts to obtain more detailed HRTEM images of these unique low dimensional systems. The results of these theoretical and experimental studies will be reported on elsewhere.

ACKNOWLEDGMENTS

The authors would like to thank M. L. H. Green for his advice in the preparation of this manuscript and the EPSRC for financial support (GR/S83968/01). J.C.G. would like to

thank the Oxford Supercomputer Center for support and computing facilities. E.L.S. would like to thank E. Artacho and M. Pruneda for assistance in the implementation and application of the SIESTA code.

*Author to whom correspondence should be addressed. Electronic address: jennifer.green@chem.ox.ac.uk

- ¹S. Iijima, *Nature (London)* **354**, 56 (1991).
- ²S. Iijima and T. Ichihashi, *Nature (London)* **363**, 603 (1993).
- ³M. S. Dresselhaus, G. Dresselhaus, and R. Saito, *Physical Properties of Carbon Nanotubes* (Imperial College, London, 1998).
- ⁴M. S. Dresselhaus, G. Dresselhaus, and R. Saito, *Carbon* **33**, 883 (1995).
- ⁵M. S. Dresselhaus, G. Dresselhaus, J. C. Charlier, and E. Hernandez, *Philos. Trans. R. Soc. London, Ser. A* **362**, 2065 (2004).
- ⁶C. T. White and J. W. Mintmire, *J. Phys. Chem. B* **109**, 52 (2005).
- ⁷P. L. McEuen, *Nature (London)* **393**, 15 (1998).
- ⁸A. P. Graham, G. S. Duesberg, W. Hoenlein, F. Kreupl, M. Liebau, R. Martin, B. Rajasekharan, W. Pamler, R. Seidel, W. Steinhögl, and E. Unger, *Appl. Phys. A* **A80**, 1141 (2005).
- ⁹M. Liebau, A. P. Graham, G. S. Duesberg, E. Unger, R. Seidel, and F. Kreupl, *Fullerenes, Nanotubes, Carbon Nanostruct.* **13**, 255 (2005).
- ¹⁰R. H. Baughman, A. A. Zakhidov, and W. A. de Heer, *Science* **297**, 787 (2002).
- ¹¹W. A. de Heer, *Mater. Res. Bull.* **29**, 281 (2004).
- ¹²M. Valcarcel, B. M. Simonet, S. Cardenas, and B. Suarez, *Anal. Bioanal. Chem.* **382**, 1783 (2005).
- ¹³M. Endo, T. Hayashi, Y. A. Kim, M. Terrones, and M. S. Dresselhaus, *Philos. Trans. R. Soc. London, Ser. A* **362**, 2223 (2004).
- ¹⁴S. Reich, C. Thomsen, and J. Maultzsch, *Carbon Nanotubes: Basic Concepts and Physical Properties* (Wiley-VCH, Weinheim, 2004).
- ¹⁵A. Kukovec, T. Pichler, R. Pfeiffer, C. Kramberger, and H. Kuzmany, *Phys. Chem. Chem. Phys.* **5**, 582 (2003).
- ¹⁶L. Grigorian, G. U. Sumanasekera, A. L. Loper, S. Fang, J. L. Allen, and P. C. Eklund, *Phys. Rev. B* **58**, R4195 (1998).
- ¹⁷P. Petit, C. Mathis, C. Journet, and P. Bernier, *Chem. Phys. Lett.* **305**, 370 (1999).
- ¹⁸A. Penicaud, P. Poulin, A. Derre, E. Anglaret, and P. Petit, *J. Am. Chem. Soc.* **127**, 8 (2005).
- ¹⁹R. S. Lee, H. J. Kim, J. E. Fischer, A. Thess, and R. E. Smalley, *Nature (London)* **388**, 255 (1997).
- ²⁰A. M. Rao, P. C. Eklund, S. Bandow, A. Thess, and R. E. Smalley, *Nature (London)* **388**, 257 (1997).
- ²¹S.-H. Jhi, S. G. Louie, and M. L. Cohen, *Solid State Commun.* **123**, 495 (2002).
- ²²N. Park, D. Sung, S. Hong, D. Kang, and W. Park, *Physica E (Amsterdam)* **29**, 693 (2005).
- ²³L.-J. Li, A. N. Khlobystov, J. G. Wiltshire, G. A. D. Briggs, and R. J. Nicholas, *Nat. Mater.* **4**, 481 (2005).
- ²⁴L. Guan, Z. Shi, M. Li, and Z. Gu, *Carbon* **43**, 2780 (2005).
- ²⁵J. Lu, S. Nagase, D. Yu, H. Ye, R. Han, Z. Gao, S. Zhang, and L. Peng, *Phys. Rev. Lett.* **93**, 116804 (2004).
- ²⁶T. Takenobu, T. Takano, M. Shiraishi, Y. Murakami, M. Ata, H. Kataura, Y. Achiba, and Y. Iwasa, *Nat. Mater.* **2**, 683 (2003).
- ²⁷R. J. Baierle, S. B. Fagan, R. Mota, A. J. R. da Silva, and A. Fazzio, *Phys. Rev. B* **64**, 085413 (2001).
- ²⁸S. B. Fagan, R. Mota, A. J. R. Da Silva, and A. Fazzio, *J. Phys.: Condens. Matter* **16**, 3647 (2004).
- ²⁹M. M. Rahman, M. Kisaku, T. Kishi, D. Matsunaka, W. A. Dino, H. Nakanishi, and H. Kasai, *J. Phys.: Condens. Matter* **16**, S5755 (2004).
- ³⁰W. Y. Choi, J. W. Kang, and H. J. Hwang, *Phys. Rev. B* **68**, 193405 (2003).
- ³¹S. B. Fagan, A. G. Souza Filho, J. Mendes Filho, P. Corio, and M. S. Dresselhaus, *Chem. Phys. Lett.* **406**, 54 (2005).
- ³²K. Hirahara, K. Suenaga, S. Bandow, H. Kato, T. Okazaki, H. Shinohara, and S. Iijima, *Phys. Rev. Lett.* **85**, 5384 (2000).
- ³³S. B. Fagan, R. Mota, A. J. R. da Silva, and A. Fazzio, *Phys. Rev. B* **67**, 205414 (2003).
- ³⁴B. W. Smith, M. Monthieux, and D. E. Luzzi, *Nature (London)* **396**, 323 (1998).
- ³⁵B. W. Smith, R. M. Russo, S. B. Chikkannanavar, and D. E. Luzzi, *J. Appl. Phys.* **91**, 9333 (2002).
- ³⁶D. J. Hornbaker, S. J. Kahng, S. Misra, B. W. Smith, A. T. Johnson, E. J. Mele, D. E. Luzzi, and A. Yazdani, *Science* **295**, 828 (2002).
- ³⁷J. Sloan, A. I. Kirkland, J. L. Hutchison, and M. L. H. Green, *Chem. Commun. (Cambridge)* **2002**, 1319.
- ³⁸J. Sloan, J. Hammer, M. Zwiefka-Sibley, and M. L. H. Green, *Chem. Commun. (Cambridge)* **1998**, 347.
- ³⁹P. M. Ajayan and S. Iijima, *Nature (London)* **361**, 333 (1993).
- ⁴⁰J. Sloan, D. M. Wright, S. Bailey, G. Brown, A. P. E. York, K. S. Coleman, M. L. H. Green, J. L. Hutchison, and H.-G. Woo, *Chem. Commun. (Cambridge)* **1999**, 699.
- ⁴¹P. M. Ajayan, O. Stephan, P. Redlich, and C. Colliex, *Nature (London)* **375**, 564 (1995).
- ⁴²R. R. Meyer, J. Sloan, R. E. Dunin-Borkowski, A. I. Kirkland, M. C. Novotny, S. R. Bailey, J. L. Hutchison, and M. L. H. Green, *Science* **289**, 1324 (2000).
- ⁴³J. Sloan, M. C. Novotny, S. R. Bailey, G. Brown, C. Xu, V. C. Williams, S. Friedrichs, E. Flahaut, R. L. Callender, A. P. E. York, K. S. Coleman, M. L. H. Green, R. E. Dunin-Borkowski, and J. L. Hutchison, *Chem. Phys. Lett.* **329**, 61 (2000).
- ⁴⁴J. Sloan, A. I. Kirkland, J. L. Hutchison, and M. L. H. Green, *Acc. Chem. Res.* **35**, 1054 (2002).
- ⁴⁵J. Sloan, D. E. Luzzi, A. I. Kirkland, J. L. Hutchison, and M. L. H. Green, *Mater. Res. Bull.* **29**, 265 (2004).
- ⁴⁶C. Yam, C. Ma, X. Wang, and G. Chen, *Appl. Phys. Lett.* **85**, 4484 (2004).
- ⁴⁷M. Wilson and P. A. Madden, *J. Am. Chem. Soc.* **123**, 2101 (2001).
- ⁴⁸M. Wilson, *J. Chem. Phys.* **116**, 3027 (2002).

- ⁴⁹M. Wilson, Chem. Phys. Lett. **366**, 504 (2002).
- ⁵⁰S. Y. Wu and C. S. Jayanthi, Phys. Rep. **358**, 1 (2002).
- ⁵¹C. F. Guerra, J. G. Snijders, G. Te Velde, and E. J. Baerends, Theor. Chem. Acc. **99**, 391 (1998).
- ⁵²P. Ordejon, Comput. Mater. Sci. **12**, 157 (1998).
- ⁵³S. Goedecker, Rev. Mod. Phys. **71**, 1085 (1999).
- ⁵⁴R. G. Parr and W. Yang, *Density-Functional Theory of Atoms and Molecules* (Oxford University Press, Oxford, 1989).
- ⁵⁵T. Ziegler, Chem. Rev. (Washington, D.C.) **91**, 651 (1991).
- ⁵⁶W. Kohn, A. D. Becke, and R. G. Parr, J. Phys. Chem. **100**, 12974 (1996).
- ⁵⁷J. M. Soler, E. Artacho, J. D. Gale, A. Garcia, J. Junquera, P. Ordejon, and D. Sanchez-Portal, J. Phys. Chem. **14**, 2745 (2002).
- ⁵⁸J. P. Perdew, K. Burke, and M. Ernzerhof, Phys. Rev. Lett. **77**, 3865 (1996).
- ⁵⁹See EPAPS Document No. E-PRBMDO-73-003616 for a full description of the pseudopotentials and basis sets used here. Calculation of the zero-point corrected bulk modulus of KI, structural parameters for KI crystals, KI@SWNT and other computational details are also provided. This document can be reached via a direct link in the online article's HTML reference section or via the EPAPS homepage (<http://www.aip.org/pubservs/epaps.html>).
- ⁶⁰D. R. Hamann, M. Schluter, and C. Chiang, Phys. Rev. Lett. **43**, 1494 (1979).
- ⁶¹M. T. Yin and M. L. Cohen, Phys. Rev. B **25**, 7403 (1982).
- ⁶²M. L. Cohen, Int. J. Quantum Chem. **61**, 603 (1997).
- ⁶³N. Troullier and J. L. Martins, Phys. Rev. B **43**, 1993 (1991).
- ⁶⁴J. B. Mann, *Atomic Structure Calculations. I. Hartree-Fock Energy Results for the Elements Hydrogen to Lawrencium* (Los Alamos Scientific Laboratories, Los Alamos, 1967).
- ⁶⁵M. A. Iron, M. Oren, and J. M. L. Martin, Mol. Phys. **101**, 1345 (2003).
- ⁶⁶A. Schulz, B. J. Smith, and L. Radom, J. Phys. Chem. A **103**, 7522 (1999).
- ⁶⁷W. B. England, Chem. Phys. **53**, 1 (1980).
- ⁶⁸S. G. Louie, S. Froyen, and M. L. Cohen, Phys. Rev. B **26**, 1738 (1982).
- ⁶⁹J. Junquera, O. Paz, D. Sanchez-Portal, and E. Artacho, Phys. Rev. B **64**, 235111 (2001).
- ⁷⁰O. F. Sankey and D. J. Niklewski, Phys. Rev. B **40**, 3979 (1989).
- ⁷¹D. Porezag, T. Frauenheim, T. Kohler, G. Seifert, and R. Kaschner, Phys. Rev. B **51**, 12947 (1995).
- ⁷²A. P. Horsfield, Phys. Rev. B **56**, 6594 (1997).
- ⁷³H. J. Monkhorst and J. D. Pack, Phys. Rev. B **13**, 5188 (1976).
- ⁷⁴F. D. Murnaghan, Proc. Natl. Acad. Sci. U.S.A. **30**, 244 (1944).
- ⁷⁵M. Bockstedte, A. Kley, J. Neugebauer, and M. Scheffler, Comput. Phys. Commun. **107**, 187 (1997).
- ⁷⁶The relation between the lattice parameter (a) and unit cell volume (V) for a fcc system is defined as $V = \frac{1}{4}a^3$.
- ⁷⁷P. Cortona, Phys. Rev. B **46**, 2008 (1992).
- ⁷⁸R. Gaudoin and W. M. C. Foulkes, Phys. Rev. B **66**, 052104 (2002).
- ⁷⁹C. N. Louis and K. Iyakutti, Phys. Status Solidi B **233**, 339 (2002).
- ⁸⁰K. Asaumi, T. Suzuki, and T. Mori, Phys. Rev. B **28**, 3529 (1983).
- ⁸¹P. Fulde, *Electron Correlations in Molecules and Solids in Solid-State Sciences* (Springer, New York, 1993), Vol. 100, p. 422.
- ⁸²Anomalous results are observed for the KI bond lengths B of supercells for which $n=19$. These anomalies result in an increase in the A/B ratio for the molecular supercell (to ~ 1.02) and a decrease in the A/B ratio (to ~ 1.00) for the infinite supercell.
- ⁸³H. Pan, Y. P. Feng, and J. Y. Lin, Phys. Rev. B **70**, 245425 (2004).
- ⁸⁴G. Sun, J. Kuerti, M. Kertesz, and R. H. Baughman, J. Phys. Chem. B **107**, 6924 (2003).